Phonon Fingerprints of CsPb$_2$Br$_5$ Single Crystals

V. G. Hadjiev,[1, 2, *] C. Wang,[3, 4] Y. Wang,[3, 5] X. Su,[3, 6] H. A.
Calderon,[7] F. Robles Hernandez,[8] Z. M. Wang,[5] and J. M. Bao[3, 5, 9]

[1] *Texas Center for Superconductivity, University of Houston, Houston, Texas 77204, USA*
[2] *Department of Mechanical Engineering, University of Houston, Houston, Texas 77204, USA*
[3] *Department of Electrical and Computer Engineering,*
University of Houston, Houston, Texas 77204, United States
[4] *Institute of Optoelectronic Information Material, School of Material Science and Engineering,*
Yunnan University, Kunming, Yunnan 650091, China
[5] *Institute of Fundamental and Frontier Sciences,*
University of Electronic Science and Technology of China, Chengdu, Sichuan 610054, China
[6] *School of Materials Science and Engineering, Chang'an University, Xi'an, Shaanxi 710061, China*
[7] *Instituto Politécnico Nacional, ESFM, Departamento de Ciencia de Materiales, UPALM, CDMX 07338, Mexico*
[8] *Mechanical Engineering Technology, University of Houston, Houston, TX 77204, United States*
[9] *Materials Science & Engineering, University of Houston, Houston, Texas 77204, United States*
(Dated: February 8, 2018)

CsPb$_2$Br$_5$ is a stable, water-resistant, material derived from CsPbBr$_3$ perovskite and featuring two-dimensional Pb-Br framework separated by Cs layers. Both compounds can coexist at nanolength scale, which often produces conflicting optical spectroscopy results. We present a complete set of polarized Raman spectra of nonluminescent CsPb$_2$Br$_5$ single crystals that reveals the symmetry and frequency of nondegenerate Raman active phonons accessible from the basal (001) plane. The experimental results are in good agreement with density functional perturbation theory simulations, which suggests that the calculated frequencies of yet unobserved double degenerate Raman and infrared phonons are also reliable. Unlike CsPbBr$_3$, the lattice dynamics of CsPb$_2$Br$_5$ is stable as evidenced by the calculated phonon dispersion. The sharp Raman lines and lack of a dynamic-disorder-induced central peak in the spectra at room temperature indicate that the coupling of Cs anharmonic motion to Br atoms, known to cause the dynamic disorder in CsPbBr$_3$, is absent in CsPb$_2$Br$_5$.

I. INTRODUCTION

Cs-based lead halide perovskites have emerged as more temperature stable optoelectronic materials than the hybrid organic-inorganic perovskite counterparts.[1] The latter are notable for their impressive power photoconversion efficiency of $> 20\%$,[2] and potential applications as light emitting diodes[3] and thermoelectrics[4]. Hybrid organic-inorganic and all-inorganic perovskites have comparable photovoltaic performance.[5] On the downside, both types of materials are water sensitive. In presence of water, CH$_3$NH$_3$PbI$_3$ degrades or forms hydrites[6] and CsPbBr$_3$ turns into CsPb$_2$Br$_5$[7]. CsPb$_2$Br$_5$ is a water-resistant material[7,8] akin to the brightly photoluminescent (PL) CsPbBr$_3$[9] but differing from the perovskites with its two-dimensional (2D) Pb-Br framework separated by Cs layers.[10] Both compounds are found or intentionally prepared to coexists at nanolength scale.[11,8] The corresponding nanocomposites[11] and CsPbBr$_3$/CsPb$_2$Br$_5$ core/shell nanostructures[8] show stable PL and structural integrity. As to the PL properties of CsPb$_2$Br$_5$, reports are controversial: from emitting strong visible PL and even lasing capabilities[12] to inherent PL inactivity[13,14]. Visible PL was observed in nanocrystalline CsPb$_2$Br$_5$[15] and in nanoplatelets[16]. On the other hand, Refs. 13 and 17 report lack of PL in CsPb$_2$Br$_5$ nanocubes and single crystals, respectively. The PL controversy stems from the fact that CsPb$_2$Br$_5$ is

an indirect band gap ($E_g \approx 3$ eV) semiconductor[13],[14],[17] that is not supposed to emit PL in the range of 2.35–2.40 eV[12],[15],[16]. A common trend in these experimental observations is that the forbidden PL in CsPb$_2$Br$_5$ is seen in nanostructures with complex morphology. The reasons for that could be remnant CsPbBr$_3$ embedded in CsPb$_2$Br$_5$, defects, crystal edge states or an interphase between the two materials. In most cases, attempts were made to resolve the controversy using x-ray diffraction (XRD) and differences in PL emissions of CsPb$_2$Br$_5$ and CsPbBr$_3$, but ambiguity remains.

One of the pressing issues is to reconcile the results of DFT modeling, that is, the wide band gap and lack of reasons for emitting PL, with a particular crystal state of CsPb$_2$Br$_5$. The potential of Raman spectroscopy to resolve this problem has not been fully explored yet as only the Raman spectra of CsPbBr$_3$ are known[18] but not those of CsPb$_2$Br$_5$. CsPbBr$_3$ undergoes two structural phase transitions with temperature: from cubic $Pm\bar{3}m$ to tetragonal $P4/mbm$ at 403 K, and further to orthorhombic $Pbnm$ at 361 K[19]. Although at room temperature CsPbBr$_3$ is already in the lowest temperature phase, its Raman spectra show broad smeared phonon peaks and scattering background in a shape of a central peak (centered at zero cm^{-1} Raman shift).[18] The perovskite structure of CsPbBr$_3$ consists of apex-to-apex connected PbBr$_6$ octahedra in a 3D framework. A combined Raman and molecular dynamics (MD) simulation study[18] of CsPbBr$_3$ show that the central peak is due to

dynamic-disorder scattering from a head-to-head Cs anharmonic motion coupled to Br face expansion of $PbBr_6$ octahedra. The 2D Pb-Br framework in $CsPb_2Br_5$ is not connected along the c-axis but separated by Cs layers. Thus if the dynamic-disorder scattering mechanism proposed in Ref. 18 is viable then we should not expect a central peak because Pb-Br layers in $CsPb_2Br_5$ lack bridging Br atoms.

In this work, we present an original Raman study of $CsPb_2Br_5$ aimed to reveal the intrinsic vibrational properties of PL inactive single crystals. A complementary density-functional perturbation theory (DFPT) simulation was carried out for calculating the lattice dynamics in $CsPb_2Br_5$ and thereby to confirm the reliability of Raman experiment and structural purity of $CsPb_2Br_5$ crystals. We also predict the phonon frequencies of Raman active modes not seen yet experimentally because of crystal morphology constraints.

II. MATERIAL PREPARATION, CHARACTERIZATION, AND RAMAN EXPERIMENT

$CsPb_2Br_5$ microplatelets were grown by conversion of $CsPbBr_3$ in pure water.[7] $CsPbBr_3$ powders (microcubes) were first synthesized using a modified method by mixing 0.5 M $Pb(CH_3COO)_2 \cdot 3H_2O$ and 1 M CsBr in 48% HBr solution at room temperature.[7,20] $CsPb_2Br_5$ was then synthesized by simply dropping $CsPbBr_3$ microcubes in large quantity of water in a flask at room temperature. Orange $CsPbBr_3$ quickly turned into white and precipitates at the bottom of the flask. The white precipitates, consisting of mainly platelet crystals, were taken out and dried for further study. XRD measurements revealed very pure phases of initial $CsPbBr_3$ and precipitated $CsPb_2Br_5$ materials.[7,20]

The Raman scattering spectra of $CsPb_2Br_5$ were measured with a Horiba JY T64000 triple spectrometer on samples placed in an Oxford Instruments Microstat^{He} optical cryostat. All spectra were recorded in backscattering configurations with incident and scattered light propagating normal to the $CsPb_2Br_5$ crystal platelet surfaces. The backscattering configurations are given in Porto's notation: $A(BC)\bar{A}$, where A and $\bar{A}$ are the propagation directions of incident and scattered light, respectively, and B and C are the corresponding light polarizations $\vec{e}_i$ and $\vec{e}_s$.

III. EXPERIMENTAL RESULTS

$CsPb_2Br_5$ crystalizes in a body-centered tetragonal structure,[10] space group $I4/mcm$ (No. 140), with lattice parameters typically close to those originally reported in Ref. 21. The $CsPb_2Br_5$ crystals adopt a platelet morphology with large faces parallel to the crystallographic (001) plane.[10] The primitive unit cell (PC) contains two

formula units of $CsPb_2Br_5$, $N_{cell} = 16$ atoms per PC with $3N_{cell} = 48$ degrees of vibrational freedom. The irreducible representations of the Γ-point phonon modes are $3A_{1g}+2B_{1g}+3B_{2g}+5E_g+2A_{1u}+5A_{2u}+3B_{1u}+B_{2u}+8E_u$, and only the A_{1g}, B_{1g}, B_{2g}, and E_g phonons are Raman active.[22] The acoustic modes have A_{2u} and E_u symmetry, whereas A_{1u}, B_{1u}, and B_{2u} are neither IR nor Raman active. The remaining $4A_{2u}$ and $7E_u$ modes can be observed in far-IR spectroscopy experiments. The Raman tensor, $\Re_S = |\alpha_{ij}|$ with $i, j = x, y, z$, of active modes $S = A_{1g}, B_{1g}, B_{2g}, E_g$, has the following non-zero components: $\Re_{A_{1g}}(\alpha_{xx} = \alpha_{yy} = a, \alpha_{zz} = b)$, $\Re_{B_{1g}}(\alpha_{xx} = -\alpha_{yy} = c)$, $\Re_{B_{2g}}(\alpha_{xy} = \alpha_{yx} = d)$, $\Re_{E_{g,1}}(\alpha_{yz} = \alpha_{zy} = e)$, and $\Re_{E_{g,2}}(\alpha_{xz} = \alpha_{zx} = -e)$.[22] The analysis of Raman scattering activity $I_S = [\vec{e}_s \cdot \Re_S \cdot \vec{e}_i]^2$ suggests that measurements in four back scattering configurations from the surface of a $CsPb_2Br_5$ platelet are enough to determine the symmetry of nondegenerate phonons. These are $Z(XY)\bar{Z}$ with $I_{B_{2g}} \neq 0$, $Z(X'X')\bar{Z}$ with $I_{A_{1g}} \neq 0$ and $I_{B_{2g}} \neq 0$, $Z(X'Y')\bar{Z}$ with $I_{B_{1g}} \neq 0$, and $Z(XX)\bar{Z}$ with $I_{A_{1g}} \neq 0$ and $I_{B_{1g}} \neq 0$, where Z and Z' are parallel to [001] crystallographic direction, X is along [100] and orthogonal to Y, X' and Y' denote [110] and [1$\bar{1}$0] directions, respectively.
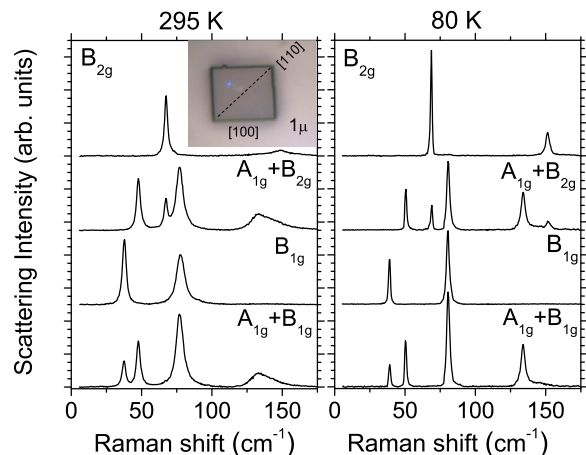

FIG. 1. (Color online) Raman spectra of the $CsPb_2Br_5$ single crystal shown in the inset, excited with 632.8 nm laser line and measured in backscattering configurations with the laser beam propagation direction along [001]. The crystal thickness is 0.5 μm. The incident ($\vec{e}_i$) and scattered ($\vec{e}_s$) light polarization directions select B_{2g} ($\vec{e}_i \parallel$ [100]; $\vec{e}_s \parallel$ [010]), $A_{1g} + B_{2g}$ ($\vec{e}_i \parallel$ [110]; $\vec{e}_s \parallel$ [110]), B_{1g} ($\vec{e}_i \parallel$ [110]; $\vec{e}_s \parallel$ [1$\bar{1}$0]), and $A_{1g} + B_{1g}$ ($\vec{e}_i \parallel$ [100]; $\vec{e}_s \parallel$ [100]).

Figure 1 shows the polarized Raman spectra of the $CsPb_2Br_5$ crystal displayed in the inset, measured in backscattering configurations from (001) crystal face. As seen in Fig. 1, the symmetry of A_{1g}, B_{1g}, and B_{2g} phonons is experimentally well established. The high single crystal quality of the sample is evidenced by the strongly polarized Raman spectra. The Raman spectra taken from a number of other $CsPb_2Br_5$ crystals including those immersed in water support the phonon sym-

metry presented in Fig. 1. The frequency of all Raman phonons measured at 80 K are listed in Table I. Notably, one B_{2g} mode is missing in the strongly polarized Raman data. Having detected only two B_{2g} phonons may confuse their symmetry assignment with that of the B_{1g} modes. The results of DFPT calculations given in Table I, however, are very helpful in this case and confirm the mode assignment in Fig. 1. As expected, none of the E_g modes were observed in the measured crystal due to the platelet crystal morphology.

The measured $CsPb_2Br_5$ crystal show no PL emission in the visible light range in accordance with the calculated electronic band structure featuring a wide indirect band gap of ≈ 3 eV.[13],[17],[14] Thus we correlate the lack of PL emission to the single crystal nature of $CsPb_2Br_5$ sample. Similar conclusions are also done in Ref. 17.

TABLE I. Experimental and DFPT Raman (R) and infrared (IR) phonon frequencies in $CsPb_2Br_5$ calculated using PAW and NC pseudopotentials. The corresponding lattice constants are $a = b = 8.38$ Å and $c = 15.27$ Å (PAW) and $a = b = 8.31$ Å and $c = 15.26$ Å (NC). TO/LO splitting of E_u modes is given for a phonon wavevector $\mathbf{q} \to 0$ along Γ-M in the Brillouin zone.

mode sym.	exp. 80 K	PAW Γ-point	NC Γ-point	mode sym.	PAW Γ-point	PAW $\mathbf{q} \to 0$ along Γ-M TO/LO
R	cm^{-1}	cm^{-1}	cm^{-1}	IR	cm^{-1}	cm^{-1}
A_{1g}	51	54	55	A_{2u}	58	59
A_{1g}	81	82	83	A_{2u}	73	73
A_{1g}	134	132	132	A_{2u}	91	94
B_{1g}	39	41	42	A_{2u}	141	153
B_{1g}	80	77	77	E_u	18	18/38
B_{2g}	69	69	71	E_u	46	46/53
B_{2g}		95	92	E_u	60	60/64
B_{2g}	152	148	147	E_u	73	73/84
E_g		36	31	E_u	95	95/106
E_g		56	52	E_u	112	112/116
E_g		70	64	E_u	131	131/135
E_g		78	76			
E_g		114	113			

IV. DFPT CALCULATION DETAILS

The DFPT lattice dynamics calculations of $CsPb_2Br_5$ were performed within the generalized-gradient approximation (GGA) with PBEsol functional[23] using the DFPT code[24] as implemented in the Quantum Espresso (QE) suite[25]. In the calculations, we used the projector-augmented-wave (PAW) approach[26] with pseudopotentials generated[27] for use with QE. The geometry optimization of crystal structure, electronic band structure, and related properties were calculated self-consistently (SCF) with 75 Ry kinetic energy cutoff for the plane wave, 300 Ry charge density cut-off, SCF tolerance better than 10^{-11}, and 5.10^{-6} Ry/au total residual force on
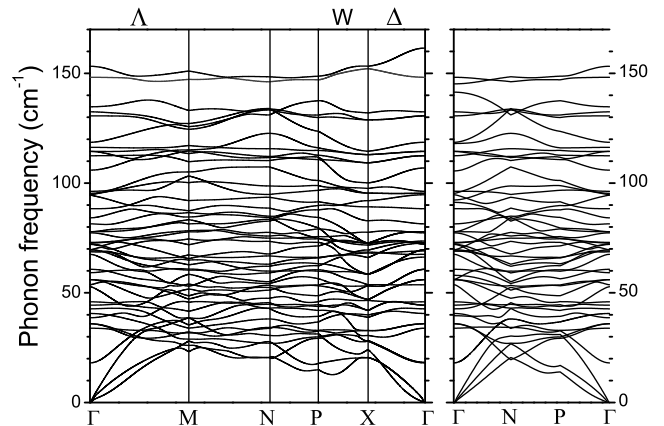

FIG. 2. DFPT calculated phonon dispersion in $CsPb_2Br_5$ with TO/LO splitting included.

atoms over $4 \times 4 \times 4$ Monkhorst-Pack (MP) k-point grid. The dynamical matrices were calculated over $4 \times 4 \times 4$ MP q-point grid and used after that for constructing the force constant matrix. Initial attempts to simulate the lattice dynamics of $CsPb_2Br_5$ at lower density k- and q-point grids produced phonon dispersions with imaginary frequencies thus implying possible inherent lattice instabilities as those seen in $CsPbBr_3$. However, increasing the density of both grids, although becoming quite computational demanding, resulted in a stable lattice dynamics with calculated Γ-phonon frequencies in a very good agreement with the low temperature experiment. The lattice constants calculated for the fully relaxed structure of $CsPb_2Br_5$ are $a = b = 8.38$ Å and $c = 15.27$ Å. The DFPT calculations relax the size and shape of crystallographic unit cell through minimization of all quantum mechanical forces in a static lattice, that is, at T=0 K. The calculated lattice constants are in a good agrement with the experimental ones measured at room temperature: $a = b = 8.48$ Å and $c = 15.25$ Å[21]. We explored multiple combinations of functionals and pseudopotentials in the calculations of lattice dynamics of $CsPb_2Br_5$ but none gave results as close to the experiment as those produced by the GGA-PBEsol-PAW scheme. Only the calculations using the norm-conserved (NC) PBESol pseudopotentials gave reasonable values for the lattice constants, $a = b = 8.31$ Å and $c = 15.26$ Å, and Γ-point phonon frequencies (e.g. see Table I) but failed to produce a stable phonon dispersion. We purposely used another DFPT code[28],[29] to calculate the non-resonant Raman intensity[30] using GGA-PBEsol-NC scheme as no such capability is available in QE.

V. DISCUSSION

Figure 2 displays the phonon dispersion of $CsPb_2Br_5$ calculated using GGA-PBESol-PAW. The TO/LO split-
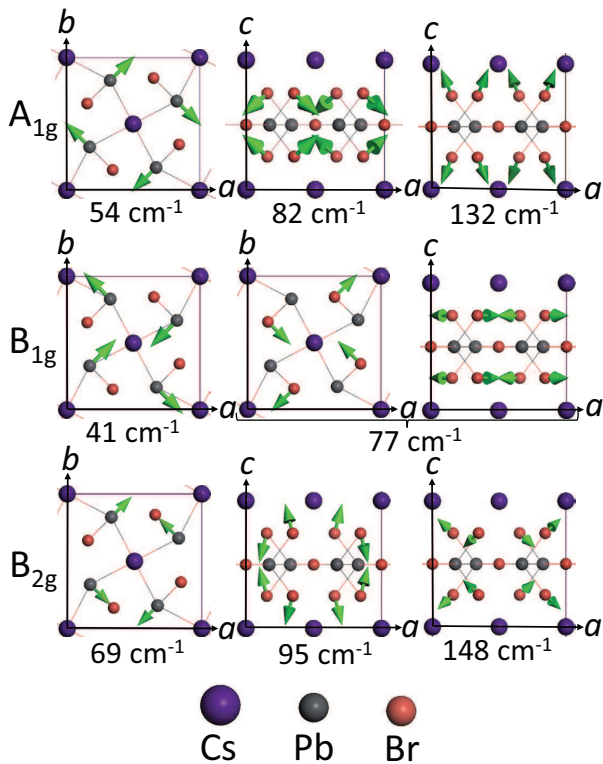
FIG. 3. (Color online) Calculated atomic displacements for the non-degenerate Raman modes in $CsPb_2Br_5$. The axes a, b, and c are along the crystallographic directions [100], [010], and [001], respectively.

ting of E_u modes at Γ-point is also accounted for phonon propagation towards the Brillouin zone boundaries points $M(\frac{1}{2}, \frac{1}{2}, -\frac{1}{2})$, $X(0, 0, \frac{1}{2})$, $N(0, \frac{1}{2}, 0)$, and $P(\frac{1}{4}, \frac{1}{4}, \frac{1}{4})$ given in the primitive basis. The phonon dispersion in Fig. 2 displays phonon bands that are closely spaced in frequency and have to be resolved by their eigenvectors. This is one of the reasons for making the lattice dynamics calculations of $CsPb_2Br_5$ difficult and unstable. In addition, the out-of-plane acoustic modes in 2D materials have quadratic dispersion and tend to produce negative frequencies around Γ-point if the fast Fourier transformation grid is not dense enough as shown in Ref. 31 for $CsPb_2Br_5$ slab calculations. The quadratic dispersion effect in Fig. 2 is seen in the flattening of one of the acoustic modes most pronounced at Γ-point along the Γ-P and Γ-X directions.

As seen in Fig. 1 the predicted B_{2g} mode at 95 cm^{-1} lacks measurable Raman intensity. The calculations of Raman activity $I_S(\omega) = [\vec{e}_s \cdot (\partial\tilde{\alpha}/\partial Q_i) \cdot \vec{e}_i]^2$, where $\tilde{\alpha}$ is the polarizability tensor and Q_i the normal mode coordinates, yielded $I_{B_{2g}}(95\,cm^{-1})/I_{B_{2g}}(69\,cm^{-1}) = 1.3\times10^{-3}$ and $I_{B_{2g}}(95\,cm^{-1})/I_{B_{2g}}(148\,cm^{-1}) = 8\times10^{-4}$ for the scattering configuration with $\vec{e}_i \parallel [100]$ and $\vec{e}_s \parallel [010]$. Therefore, the eigenvector of the 95 cm^{-1} mode produces vanishing modulation of the crystal polarizability.

In Fig. 3, we show the calculated atomic displacements

for all non-degenerate Raman modes in $CsPb_2Br_5$. Comparing the experimental Raman intensities in Fig. 1 with the vibrational patterns in Fig. 3 we conclude that the intensity is strong for all modes in which Br atoms move in-phase and predominantly in-plane in the Pb-Br layer. Apparently, this does not apply to the B_{2g} mode at 95 cm^{-1}.
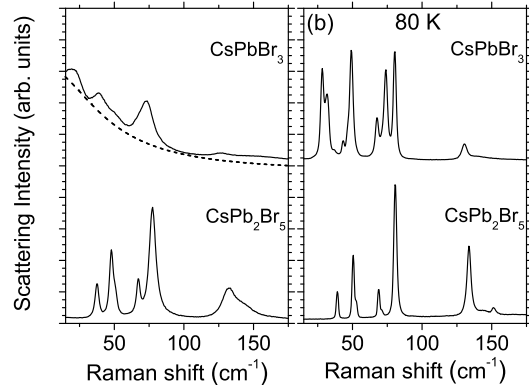

FIG. 4. Comparison of non-polarised Raman spectra of $CsPb_2Br_5$ and $CsPbBr_3$. The dash curve in (a) is a guide to the eye that depicts the dynamic-disorder-induced central peak in $CsPbBr_3$[18].

Figure 4 demonstrates the difference between the Raman spectra of $CsPb_2Br_5$ and $CsPbBr_3$ at room and low temperatures. The assignment of Raman phonons in $CsPbBr_3$ is given in Ref. 18. We note, however, that the Raman spectrum of $CsPbBr_3$ shown in Fig. 4 (b) was measured at a higher spectral resolution than that in Ref. 18 and exhibits more spectral lines although not all of the expected by symmetry considerations. The presence of small amount of $CsPbBr_3$ as an impurity in $CsPb_2Br_5$ might be challenging to detect at room temperature because of the smeared Raman features of $CsPbBr_3$. At low temperatures, however, the spectral range below 40 cm^{-1} is free of $CsPb_2Br_5$ Raman lines and the presence of $CsPbBr_3$ can be monitored through the Raman peaks at 28 cm^{-1} and 32 cm^{-1}. We believe that Fig. 4 serves as a useful reference for the material characterization of both compounds and will be helpful in detecting traces of $CsPbBr_3$ in $CsPb_2Br_5$.

VI. CONCLUSIONS

In summary, we have presented a comprehensive Raman scattering study of $CsPb_2Br_5$. The DFPT calculation results are in very good agreement with experimental phonon frequencies and symmetry. The latter gives us confidence that the calculated phonon dispersion and phonon related, yet unmeasured, properties are also accessed properly. The present Raman study give an evidence that the lack of visible PL emission is

an intrinsic property of $CsPb_2Br_5$ single crystals.

ACKNOWLEDGMENTS

---

* vhadjiev@uh.edu

[1] M. Kulbak, D. Cahen and G. Hodes, J. Phys. Chem. Lett.**6**, 2452-2456 (2015).

[2] W. S. Yang, B. W. Park, E. H. Jung, N. J. Jeon, Y. C. Kim, D. U. Lee, S. S. Shin, J. Seo, E. K. Kim, J. H. Noh, and S. I. Seok, Science **356**, 1376 (2017).

[3] S. D. Stranks and H. J. Snaith, Nat. Nanotechnl. **10**, 391 (2015).

[4] Y. He and G. Galli, Chem. Mat. **26**, 27024 (2016).

[5] M. Kulbak, S. Gupta, N. Kedem, I. Levine, T. Bendikov, G. Hodes, and D. Cahen, J. Phys. Chem. Lett. **7**, 167172 (2016).

[6] Z. Zhu, V. G. Hadjiev, Y. G. Rong, R. Guo, B. Cao, Z. J. Tang, F. Qin, Y. Li, Y. N. Wang, F. Hao, S. Venkatesan, W. Z.Li, S. Baldelli, A. M. Guloy, H. Fang, Y. D. Hu, Y. Yao, Z. M. Wang, and J. M. Bao, Chem. of Materials **28**, 7385-7393 (2016).

[7] Y. Wang, C. Wang, X. H. Su, V. G. Hadjiev, H. A. Calderon, Y. Z. Ni, M. K. Alam, F. Robles-Hernandez, Y. Yao, Y. Yang, S. Chen, Z. F. Ren, Z. M. Wang, and J. M. Bao, submitted for publication elswhere (unpublished).

[8] B. Qiao, P. Song, J. Cao, S. Zhao, Z. Shen, D. Gao, Z. Liang, Z. Xu, D. Song, and X. Xu, Nanotechnology **28**, 443602 (2017).

[9] L. Protesescu, S. Yakunin, M. I. Bondnarchuk, F. Krieg, R. Caputo, C. H. Hendon, R. X. Yang, A. Walsh, and M. V. Kovalenko, Nano Lett. **15**, 3692-3696 (2015).

[10] H. M. Powell and H. S. Tasker, J. Chem. Soc. **0**, 119-123 (1937).

[11] F. Palazon, S. Dogan, S. Marras, F. Locardi, I. Nelli, P. Rastogi, M. Ferreti, M. Pratto, R. Krahne, and L. Manna, J. of Phys. Chem. C, **121**, 11956-11961 (2017).

[12] X. Tang, Z. Hu, W. Yuan, W. Hu, H. Shao, D. Han, J. Zheng, J. hao, Z. Zang, J. Du, Y. Leng, L. Fang, and M. Zhou, Adv. Optical Mater. **5**, 1600788 (2017).

[13] G. Li, H. Wang, Z. Zhu, Y. Chang, T. Zhang, Z. Song, and Y. Jiang, Chemm. Commun. **52**, 11296-11299 (2016).

[14] Z. Zhang, Y. Zhu, W. Wang, W. Zheng, R. Lin, and F. Huang, J. Mater. Chem. C **6**, 446-451 (2018).

[15] H. Yang, Y. Zhang, J. Pan, J. Yin, O. M. Bakr, and O. F. Mohammed, Chem. Mater. **29**, 8978-8982 (2017).

[16] J. Lv, L. Fang, and J. Shen, Mat. Lett. **211**, 199-202 (2018).

[17] I. Dursun, M. De Bastiani, B. Turedi, B. Alamer, A. Shkurenko, J. Yin, A. M. El-Zohry, I. Gereige, A. AlSag-gaf, O. F. Mohammed, M. Eddaoudi, and O. M. Bakr, ChemSusChem **10**, 3746 3749 (2017).

[18] O. Yaffe, Y. S. Guo, L. Z. Tan, D. A. Egger, T. Hull, C. C. Stoumpos, F. Zheng, T. F. Heinz, L. Kronik, M. G. Kanatzidis, J. S. Owen, A. M. Rappe, M. A. Pimenta, and L. E. Brus, Phys. Rev. Lett. **118**, 136001 (2017).

[19] S. Hirotsu, J. Harada, M. Iizumi, and K. Gesi, J. Phys. Soc. Jpn. **37** 1393-1398 (1974).

[20] C. C. Stoumpos, C. D. Malliakas, J. A. Peters, Z. Liu, M. Sebastian, J. Im, T. C. Chasapis, A. C. Wibowo, D. Y. Chung, A. J. Freeman, B. W. Wessels, and M. G. Kanatzidis, Crystal Growth & Design **13**, 2722-2727 (2013).

[21] M. Cola, V. Massarotti, R. Riccardi, and C. Sinistri, Z. Naturforsch. **26**, 1328-1332 (1971).

[22] D. L. Rousseau, R. P. Bauman, and S. P. S. Porto, J. of Raman Spec. **10**, 253-290 (1981).

[23] J. P. Perdew, A. Ruzsinszky, G. I. Csonka, O. A. Vydrov, G. E. Scuseria, L. A. Constantin, X. Zhou, and K. Burke, Phys Rev Lett. **100**, 136406 (2008).

[24] S. Baroni, S. de Gironcoli, A. dal Corso, P. Giannozzi, Rev. Mod. Phys. **73**, 515 (2001).

[25] P. Giannozzi, S. Baroni, N. Bonini, M. Calandra, R. Car, C. Cavazzoni, D. Ceresoli, G. L. Chiarotti, M. Cococcioni, I. Dabo, A. Dal Corso, S. de Gironcoli, S. Fabris, G. Fratesi, R. Gebauer, U. Gerstmann, C. Gougoussis, A. Kokalj, M. Lazzeri, L. Martin-Samos, N. Marzari, F. Mauri, R. Mazzarello, S. Paolini, A. Pasquarello, L. Paulatto, C. Sbraccia, S. Scandolo, G. Sclauzero, A. P. Seitsonen,A. Smogunov, P. Umari, and R. M. Wentzcovitch, J. Phys.: Cond. Mat. **21**, 395502 (2009).

[26] P. E. Blöchl, Phys. Rev. B **50**, 17953-17979 (1994).

[27] A. Dal Corso, Comp. Mat. Science **95**, 337-350 (2014).

[28] S. J. Clark, M. D. Segall, C. J. Pickard, P. J. Hasnip, M. J. Probert, K. Refson, and M. C. Payne, Z. Kristallogr. **220**, 567-570 (2005).

[29] K. Refson, P. R. Tulip, and S. J. Clark, Phys. Rev. B **73**, 155114 (2006).

[30] D. Porezag and M. R. Pederson, Phys. Rev. B **54**, 7830 (1996).

[31] F. Iyikanat, E. Sari, and H. Sahin, Phys. Rev. B **96**, 155442 (2017).